RESEARCH ARTICLE
doi: 10.2306/scienceasia1513-1874.2025.057

ScienceAsia 51 (4): 2025: ID 2025057: **1–11**

Circular RNA ARF3 attenuates $PM_{2.5}$-induced inflammatory response in human bronchial epithelial cells by regulating microRNA-509-3p and chromodomain helicase DNA binding protein 9

Zhu Zhou, YiMei Wang, Xiang Huang, LiWen Zhang, Di Wu, Yi Ren, Fei Lu, XiKun Gao*

Intensive Care Unit, Changshu Hospital Affiliated to Nanjing University of Chinese Medicine, Jiangsu 215500 China

*Corresponding author, e-mail: cssgaoxikun@163.com

Received 19 Apr 2023, Accepted 20 Dec 2024
Available online 13 Jul 2025

ABSTRACT: The present study deciphered the molecular mechanisms by which circARF3 attenuates particulate matter 2.5 ($PM_{2.5}$)-induced bronchial epithelial cell damage. Bronchial epithelial injury was modeled by $PM_{2.5}$ exposure. To regulate circARF3, microRNA-509-3p (miR-509-3p) and Chromodomain Helicase DNA Binding Protein 9 (CHD9), plasmid transfection and oligonucleotide techniques were used. Cell viability was quantified by Cell Counting Kit-8 assay. Apoptosis rate was determined by flow cytometry, while apoptotic genes were assessed by quantitative real-time polymerase chain reaction. Reactive oxygen levels were measured using a 2′,7′-dichlorofluorescein diacetate fluorescent probe. Levels of the inflammatory cytokines were assessed by enzyme-linked immunosorbent assay, and CHD9, Toll-Like Receptor 4, and phosphorylated nuclear factor-kappa B subunit p65 were measured by Western blotting analysis. Targeted interactions between miR-509-3p, circARF3 and CHD9 were verified using dual luciferase reporter and RNA immunoprecipitation assays. Exposure to $PM_{2.5}$ decreased bronchial epithelial cell viability, increased apoptosis, and elevated ROS while activating the TLR4/NF-κB pathway. CircARF3 overexpression or knockdown inhibited and promoted $PM_{2.5}$-induced injury, respectively. Overexpressing miR-509-3p exacerbated $PM_{2.5}$-induced injury, whereas overexpressing CHD9 showed the opposite effect. CircARF3 competitively bound miR-509-3p to mediate CHD9 expression. CircARF3 attenuates $PM_{2.5}$-induced damage to bronchial epithelial cells by regulating miR-509-3p and promoting CHD9 expression.

KEYWORDS: circular RNA ARF3, microRNA-509-3p, Chromodomain Helicase DNA Binding Protein 9, particulate matter 2.5, human bronchial epithelial cells

INTRODUCTION

In the present world today, increase in human activity and chemical pollution has worsened air pollution, especially in the form of haze [1–3]. Particulate matter with an aerodynamic diameter of less than 10 micrometers (PM_{10}) and 2.5 micrometers ($PM_{2.5}$) are major constituents of this environmental issue. $PM_{2.5}$ is associated with the progression of systemic diseases, especially targeting the respiratory system [4–6]. Inhaling these particles causes cellular inflammation, oxidative stress, and apoptosis in the respiratory tract and lung epithelium [7, 8]. In spite of efforts to reduce $PM_{2.5}$ pollution, the complex mechanisms by which $PM_{2.5}$ damages respiratory epithelial cells are still unclear.

Circular RNAs (circRNAs), characterized by their unique covalently closed-loop structures, are a group of endogenous non-coding RNAs with stable expression [9]. These circRNAs have been implicated in a diverse array of diseases, including cancer [10], ischemia-reperfusion injury [11], and neurodegenerative diseases [12, 13]. Recent research has revealed the crucial role of circRNAs in respiratory system inflammation. For instance, CircRNA_0026344 modulates miR-21 and Smad7 in the epithelial-to-mesenchymal transition during cigarette smoke-induced pulmonary fibrosis [14]. Interleukin-13 induces inflammatory cytokines and mucins in nasal epithelial cells by miR-375/Krüppel-like factor 4-regulated circARRDC3 [15]. Moreover, circRNAs such as circBBS9 and circ406961 have been shown to exacerbate $PM_{2.5}$-induced respiratory epithelial cell inflammation, activating the NLR family pyrin domain containing 3 inflammasome or signal transducer and activator of transcription 3/c-Jun N-terminal kinase signaling pathways [16, 17]. ARF3 (circARF3) is well known for its anti-inflammatory effects, including the ability to reduce tumor necrosis factor alpha (TNF-α)-induced inflammation and adipose tissue inflammation [18]. However, the specific role of circARF3 in cellular damage induced by $PM_{2.5}$ exposure remains to be elucidated.

The Toll-like receptor 4/nuclear factor-kappaB (TLR4/NF-κB) signaling pathway stands as a cornerstone in the immune system, orchestrating inflammatory responses and host defense mechanisms. When $PM_{2.5}$ particles are inhaled, TLR4 serves as a pattern recognition receptor, identifying the particles and triggering cellular inflammatory responses [19]. Activated TLR4 triggers a cascade of signaling pathways such as NF-κB. As a transcription factor, NF-κB translocates to the nucleus, upregulating the expression of inflammation-related genes [20]. The upregulation

of these molecules leads to the recruitment and activation of inflammatory cells, further exacerbating airway inflammation [21]. It is thus clear that the TLR4/NF-κB pathway plays a role in $PM_{2.5}$-induced airway inflammation, and is therefore a new target for the control of severe respiratory diseases.

In this study, we delved into the role of circARF3 in bronchial epithelial cell damage induced by $PM_{2.5}$. We discovered that circARF3 attenuates inflammation, oxidative stress, and apoptosis in bronchial epithelial cells following $PM_{2.5}$ exposure. CircARF3 protects against $PM_{2.5}$-induced cellular damage primarily through interaction with miR-509-3p and CHD9, revealing a novel mechanistic insight.

MATERIALS AND METHODS

$PM_{2.5}$ preparation

Standard Reference Material $PM_{2.5}$ (SRM1648a) was procured from the National Institute of Standards and Technology (NIST, Gaithersburg, MD, USA). A stock solution of $PM_{2.5}$ at a concentration of 50 mg/ml was prepared in phosphate-buffered saline (PBS) and subjected to ultrasonication for 30 min on ice using equipment from Sonics (Newtown, PA, USA). The endotoxin content in $PM_{2.5}$ was assessed using the Toxinsensor™ Chromogenic LAL Endotoxin Assay Kit from GenScript (Piscataway, NJ, USA).

Cell culture

Human bronchial epithelial cell line BEAS-2B was acquired from Cellcook Biotech Co., Ltd. (Guangzhou, China). BEAS-2B cells were cultured in bronchial epithelial cell basal medium supplemented with BEGM components, both sourced from Lonza (Basel, Switzerland). The cells were maintained in a humidified incubator at 37 °C with 5% CO_2. Cells were seeded in culture dishes and exposed to $PM_{2.5}$ after 24 h. BEAS-2B cells were exposed to varying concentrations of $PM_{2.5}$ (0, 25, 50, 75, 100, and 125 μg/ml) for 48 h, with PBS serving as the control.

Cell transfection

Small interfering RNAs targeting circARF3 and CHD9, along with negative controls (si-circARF3, si-CHD9, and si-NC), and overexpression plasmids for circARF3 and CHD9, together with their respective negative controls (oe-circARF3, oe-CHD9, and oe-NC), were designed and synthesized by GenPharma (Shanghai, China). MiR-509-3p mimic, miR-509-3p inhibitor, mimic negative control (mimic NC), and inhibitor negative control (inhibitor NC) were purchased from RiboBio (Guangzhou, China). Plasmids and oligonucleotides were transfected into BEAS-2B cells using Lipofectamine 2000 from Invitrogen (Carlsbad, CA, USA), following the manufacturer's protocol. Cells were harvested 48 h post-transfection for subsequent experiments.

Cell viability assay

Cell viability was assessed using the Cell Counting Kit-8 (CCK-8) from Dojindo (Kumamoto, Japan). BEAS-2B cells (1×10^4) were seeded in a 96-well plate and exposed to various concentrations of $PM_{2.5}$ for 48 h. Subsequently, 10 μl of CCK-8 solution was added to each well, and optical density at 450 nm was measured after 2 h using a BioTek Epoch2 microplate reader (Winooski, VT, USA).

Flow cytometric analysis of apoptosis

Apoptosis was quantified using the FITC-Annexin V Apoptosis Detection Kit from Beyotime (Shanghai, China). Collected BEAS-2B cells were washed with PBS and stained with FITC-Annexin V (300 ng/ml at 4 °C for 10 min). Cells were then incubated with propidium iodide at 37 °C for 5 min. Data acquisition was performed using the LSRFortessa flow cytometer (BD Biosciences, San Jose, CA, USA) and analyzed using FlowJo software version 7.6.1.

Enzyme-linked immunosorbent assay (ELISA)

Levels of interleukin-6 (IL-6), IL-8, IL-1β, IL-4, IL-10, and IL-13 in cells were measured using ELISA kits from Invitrogen (Basel, Switzerland). Optical density at 450 nm was read using a ChroMate 4300 microplate reader (CA, USA).

Reactive oxygen species (ROS) detection

ROS production was measured using a ROS Assay Kit from Beyotime. Cells were washed with PBS and incubated with 10 μm of 2′,7′-dichlorofluorescin diacetate (DCFH-DA) and 2 μg/ml of Hoechst 33342 for 20 min. Fluorescence intensity was captured using a fluorescence microscope and analyzed with Image J software.

Quantitative reverse transcription polymerase chain reaction (RT-qPCR)

Cells were lysed using TRIzol reagent (Invitrogen; Thermo Fisher Scientific, Inc. Waltham, MA, USA), and RNA concentration was determined using a NanoDrop 2000 spectrophotometer. Complementary DNA (cDNA) for mRNA was synthesized using PrimeScript RT Master Mix (Takara Bio, Inc., Shiga, Japan), while cDNA for microRNA (miRNA) was synthesized using the RevertAid First Strand cDNA Synthesis kit (Thermo Fisher Scientific, Inc.). RT-qPCR was performed using the miScript SYBR® Green PCR kit (Thermo Fisher Scientific, Inc.). All assays were conducted in triplicate, with glyceraldehyde 3-phosphate dehydrogenase and U6 snRNA serving as internal controls for mRNA and miRNA, respectively. Relative gene expression levels were analyzed using the $2^{-\Delta\Delta Ct}$ method. The primers used are listed in Table S1.

Western Blot Analysis

Cells were harvested and lysed using radioimmunoprecipitation assay buffer (Beyotime). Protein concentrations were quantified using a bicinchoninic acid Protein Assay Kit (Beyotime). Proteins were then separated by 10% sodium dodecyl sulfate-polyacrylamide gel electrophoresis and transferred onto polyvinylidene fluoride membranes. The membranes were blocked with 5% non-fat milk and incubated with primary antibodies against CHD9 (13402-1-AP, Proteintech, Wuhan, China), TLR4 (ab13556, Abcam, Cambridge, UK), phosphorylated (p)-NF-κB (8242, Cell Signaling Technology, Danvers, MA, USA), and NF-κB (3031, Cell Signaling Technology). Horseradish peroxidase-conjugated secondary antibodies were added to the membranes, which were incubated at room temperature for 1 h. Chemiluminescence was detected using an enhanced chemiluminescence detection kit (P0018FS; Beyotime) and imaged with a chemiluminescent gel imaging system (Tanon-5200; Tanon Science & Technology Co., Ltd., Shanghai, China).

Dual-luciferase reporter assay

Wild-type or mutant 3′ untranslated regions (3′UTRs) of circARF3 and CHD9 containing miR-509-3p binding sites were cloned into the pMIR-REPORT vector (Ambion, Austin, TX, USA) and designated as WT/MUT-circARF3 and WT/MUT-circCHD9. BEAS-2B cells were seeded in 24-well plates and, upon reaching 80% confluence, were co-transfected with the aforementioned plasmids and miR-509-3p mimic or mimic-NC using Lipofectamine 2000. Luciferase activity was measured 24 h post-transfection using the Dual-Luciferase Reporter Assay System (Promega, Madison, WI, USA). The luciferase activity was presented as the ratio of firefly luciferase activity to Renilla luciferase activity.

RNA immunoprecipitation (RIP) experiment

The EZ-Magna RIP Kit (Millipore, Billerica, MA, USA) was employed according to the manufacturer's protocol. BEAS-2B cells were lysed and incubated with magnetic beads conjugated with anti-Argonaute2 (Ago2) antibody (Millipore). Normal mouse IgG (Millipore) served as the negative control. Samples were incubated with proteinase K, followed by RNA extraction from the immunoprecipitated complexes. The purified RNA was then analyzed by RT-qPCR.

Data analysis

Data were expressed as mean ± standard deviation (SD). Statistical analysis was performed using GraphPad Prism version 6.0 (GraphPad Software, Inc., San Diego, CA, USA). Differences between two groups were analyzed using Student's *t*-test, and differences among three or more groups were assessed using one-way analysis of variance, followed by Tukey's multiple comparisons test. A p-value < 0.05 was considered statistically significant.

RESULTS

$PM_{2.5}$ induces inflammation and apoptosis in BEAS-2B cells

To explore the effects of $PM_{2.5}$ on human bronchial epithelial cells (BEAS-2B), we subjected these cells to escalating concentrations of $PM_{2.5}$ over a 48-h exposure period. Using the CCK-8, we observed that $PM_{2.5}$ compromised BEAS-2B cell viability in a concentration-dependent manner (Fig. 1A). Concurrent flow cytometric analysis corroborated these findings, showing a surge in apoptosis levels with increasing $PM_{2.5}$ (Fig. 1B). We further investigated the oxidative and inflammatory responses in BEAS-2B cells exposed to 125 μg/ml of $PM_{2.5}$. As illustrated in Fig. 1C, treatment with $PM_{2.5}$ markedly augmented ROS levels within these cells. Subsequent ELISA assessments revealed a pronounced upregulation in the levels of the pro-inflammatory cytokines IL-1β, IL-6, and IL-8, alongside an increase in the anti-inflammatory cytokines IL-4 and IL-13. Conversely, levels of the anti-inflammatory cytokine IL-10 were notably diminished (Fig. 1D). Western blot analyses provided additional insight, demonstrating enhanced TLR4 expression and augmented phosphorylation of NF-κB p65 following $PM_{2.5}$ exposure (Fig. 1E). These data collectively suggest that $PM_{2.5}$ instigates a robust inflammatory response and apoptosis in BEAS-2B cells, underscoring its potential pathogenic impact on respiratory epithelial cell integrity.

CircARF3 regulation of $PM_{2.5}$-induced cellular responses in bronchial epithelium

To elucidate the role of circARF3 in $PM_{2.5}$-mediated cellular damage in BEAS-2B cells, we initially quantified circARF3 expression levels following $PM_{2.5}$ exposure. As depicted in Fig. 2A, $PM_{2.5}$ treatment resulted in a concentration-dependent decrease in circARF3 expression in BEAS-2B cells. Subsequent transfections with circARF3-overexpressing plasmids and siRNAs targeting circARF3 were performed (Fig. 2B). Our findings indicated that overexpression of circARF3 significantly enhanced cellular viability, whereas siRNA-mediated knockdown of circARF3 further reduced it (Fig. 2C). Flow cytometric analyses confirmed that overexpression of circARF3 led to a reduction in apoptosis rates, in contrast, knockdown of circARF3 aggravated apoptosis in these cells (Fig. 2D). Furthermore, RT-qPCR analyses showed that overexpressing circARF3 downregulated the expression of the pro-apoptotic marker Bax and upregulated the anti-apoptotic marker Bcl-2. Conversely, knockdown of circARF3 increased Bax expression and decreased Bcl-2 expression (Fig. 2E). ROS production following $PM_{2.5}$ exposure was measured using the DCFH-DA assay. Re-

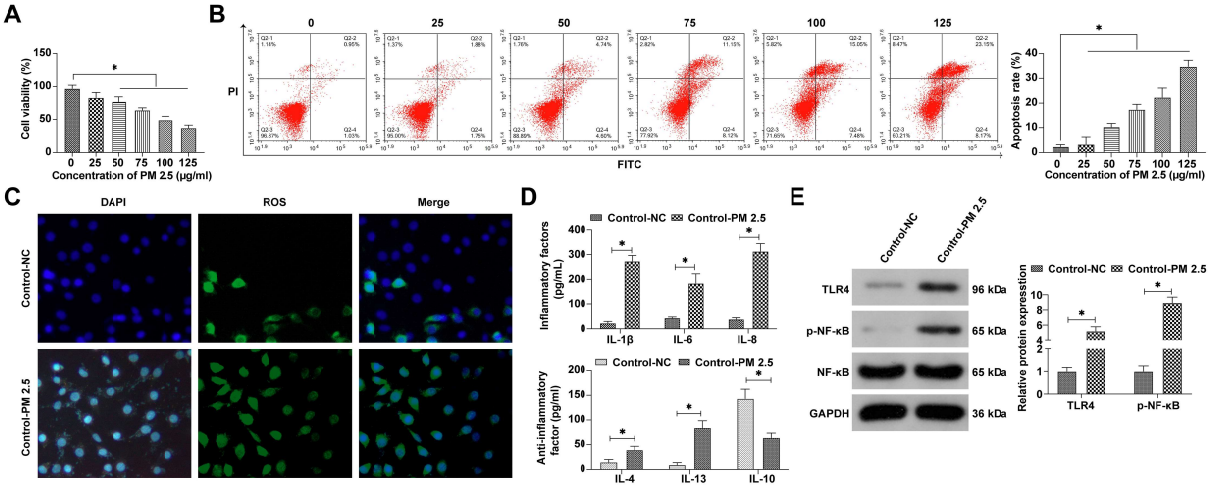

Fig. 1 $PM_{2.5}$ induces inflammation and apoptosis in human bronchial epithelial cells. A: Cell viability in BEAS-2B cells after $PM_{2.5}$ treatment at 0, 25, 50, 75, 100, and 125 μg/ml, assessed by CCK-8; B: Apoptosis rates in BEAS-2B cells post-$PM_{2.5}$ exposure at various concentrations, measured by flow cytometry; C: ROS levels in BEAS-2B cells after $PM_{2.5}$ exposure, determined by DCFH-DA probe; D: Inflammatory cytokine levels in BEAS-2B cells after $PM_{2.5}$ exposure, evaluated by ELISA; E: TLR4 and phosphorylated NF-κB p65 protein expression in BEAS-2B cells post-$PM_{2.5}$ exposure, analyzed by Western blot. Values are mean ± SD ($n = 3$); * $p < 0.05$.

sults demonstrated that overexpression of circARF3 resulted in reduced ROS production, whereas its knockdown led to an increase in ROS levels (Fig. 2F). ELISA assays revealed that overexpression of circARF3 modulated cytokine profiles by inhibiting the levels of pro-inflammatory cytokines IL-1β, IL-6, and IL-8, and enhancing the expression of the anti-inflammatory cytokines IL-4 and IL-13, while promoting IL-10 levels. In contrast, knockdown of circARF3 reversed these effects (Fig. 2G). Western blot analysis indicated that overexpression of circARF3 decreased the levels of TLR4 and phosphorylated NF-κB p65, whereas knockdown of circARF3 activated the NF-κB signaling pathway (Fig. 2H). These results underscore the pivotal role of circARF3 in modulating $PM_{2.5}$-induced injury in BEAS-2B cells.

miR-509-3p amplifies $PM_{2.5}$-induced cellular injury in BEAS-2B cells

Prior research indicates that miR-509-3p expression is elevated in airway epithelial cells stimulated by the pro-inflammatory cytokines IL-1β and TNF-α [22]. In this investigation, we examined the analogous influence of miR-509-3p on $PM_{2.5}$-induced cellular damage in BEAS-2B cells. Enhanced expression of miR-509-3p was observed in BEAS-2B cells exposed to $PM_{2.5}$ (Fig. 3A). Subsequently, these cells were transfected with miR-509-3p mimics (Fig. 3B). The results showed that miR-509-3p overexpression decreased cellular viability and increased apoptosis rates in BEAS-2B cells (Fig. 3C,D). Additionally, RT-qPCR analysis demonstrated that miR-509-3p overexpression upregulated the pro-apoptotic marker Bax and downregulated the anti-apoptotic marker Bcl-2 (Fig. 3E). Analysis with the DCFH-DA fluorescent probe revealed that miR-509-3p overexpression accelerated ROS production in BEAS-2B cells (Fig. 3F). Moreover, overexpression of miR-509-3p also heightened the levels of IL-1β, IL-6, and IL-8, as well as anti-inflammatory cytokines IL-4 and IL-13, while simultaneously enhancing the expression of TLR4 and phosphorylated NF-κB p65, yet reduced IL-10 levels (Fig. 3G,H). These findings suggest that miR-509-3p exacerbates $PM_{2.5}$-induced cellular injury in BEAS-2B cells.

CircARF3 and CHD9: Regulatory nexus in miR-509-3p mediated pathways

Following the modulation of circARF3 in BEAS-2B cells, we detected a reduction in miR-509-3p expression post-overexpression and an elevation upon knockdown, suggesting regulation by circARF3 (Fig. 4A). To investigate whether circARF3 acts as a molecular sponge for miR-509-3p, bioinformatics analysis via http://starbase.sysu.edu.cn/ revealed potential binding sites between circARF3 and miR-509-3p (Fig. 4B). Subsequent dual-luciferase reporter assays demonstrated that wild-type circARF3 significantly reduced the luciferase activity in the miR-509-3p mimic group, whereas the mutant form had no effect (Fig. 4C). Further validation was conducted through RIP experiments, which confirmed the enrichment of circARF3 and miR-509-3p in Ago2-associated immunoprecipitates compared to IgG controls (Fig. 4D), supporting the competitive binding hypothesis.

Next, we explored downstream targets of miR-509-3p, focusing on CHD9, known for its crucial

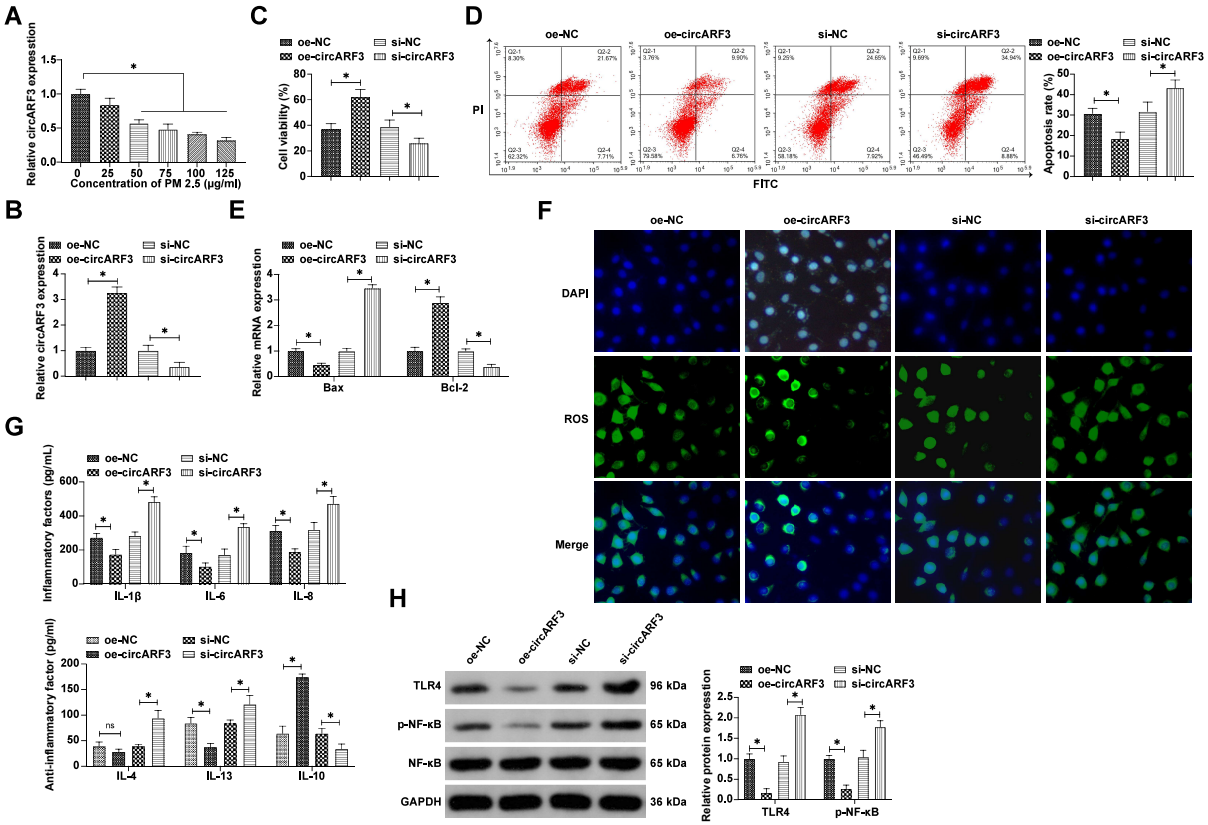

Fig. 2 CircARF3 and $PM_{2.5}$-induced inflammation and apoptosis. A: CircARF3 expression in BEAS-2B cells after $PM_{2.5}$ treatment at different concentrations; B: CircARF3 expression in BEAS-2B cells post-transfection with oe/si-circARF3; C: Cell viability in BEAS-2B cells after oe/si-circARF3 transfection; D: Apoptosis rates in BEAS-2B cells post-oe/si-circARF3 transfection; E: Bax and Bcl-2 expression in BEAS-2B cells post-oe/si-circARF3 transfection; F: ROS levels in BEAS-2B cells post-oe/si-circARF3 transfection; G: Inflammatory cytokine levels in BEAS-2B cells post-oe/si-circARF3 transfection; H: TLR4 and phosphorylated NF-κB p65 expression in BEAS-2B cells post-oe/si-circARF3 transfection. A, B, and E were assessed by RT-qPCR. C, D, F, G, and H were determined as mentioned in legend of Fig. 1. Values are mean ± SD ($n = 3$); * $p < 0.05$.

role in immune regulation as reported in previous studies [23, 24]. In our study, CHD9 expression was significantly reduced in BEAS-2B cells exposed to $PM_{2.5}$ (Fig. 4E). Moreover, overexpression of miR-509-3p markedly suppressed CHD9 expression (Fig. 4F). Predictive bioinformatics analysis via http://starbase.sysu.edu.cn/ indicated binding sites between CHD9 and miR-509-3p (Fig. 4G), suggesting that CHD9 is a target of miR-509-3p. This was further confirmed by dual-luciferase reporter assays and RIP experiments, which showed that wild-type CHD9 reduced luciferase activity in the miR-509-3p mimic group and was enriched in Ago2 immunoprecipitates (Fig. 4H,I), establishing CHD9 as a downstream target of miR-509-3p.

CHD9 overexpression mitigates $PM_{2.5}$-induced cellular injury in BEAS-2B cells

Subsequently, we explored the role of CHD9 in modulating $PM_{2.5}$-induced cellular damage in BEAS-2B cells. To this end, CHD9 overexpression plasmids were transfected into BEAS-2B cells, effectively augmenting CHD9 expression (Fig. 5A). This upregulation led to enhanced cell viability and a reduction in apoptosis rates in these cells (Fig. 5B,C). RT-qPCR analysis demonstrated that CHD9 overexpression resulted in a decrease in the pro-apoptotic gene Bax and an increase in the anti-apoptotic gene Bcl-2 (Fig. 5D). Additionally, overexpressing CHD9 significantly attenuated ROS production induced by $PM_{2.5}$ exposure (Fig. 5E). ELISA and Western blot analyses further revealed that CHD9 overexpression diminished the levels of pro-inflammatory cytokines IL-1β, IL-6, IL-8, and the anti-inflammatory cytokines IL-4 and IL-13, as well as reduced the expression of phosphorylated NF-κB p65 and TLR4 proteins. Conversely, IL-10 levels were increased (Fig. 5F,G). These findings suggest that upregulation of CHD9 expression can ameliorate $PM_{2.5}$-induced damage in BEAS-2B cells.

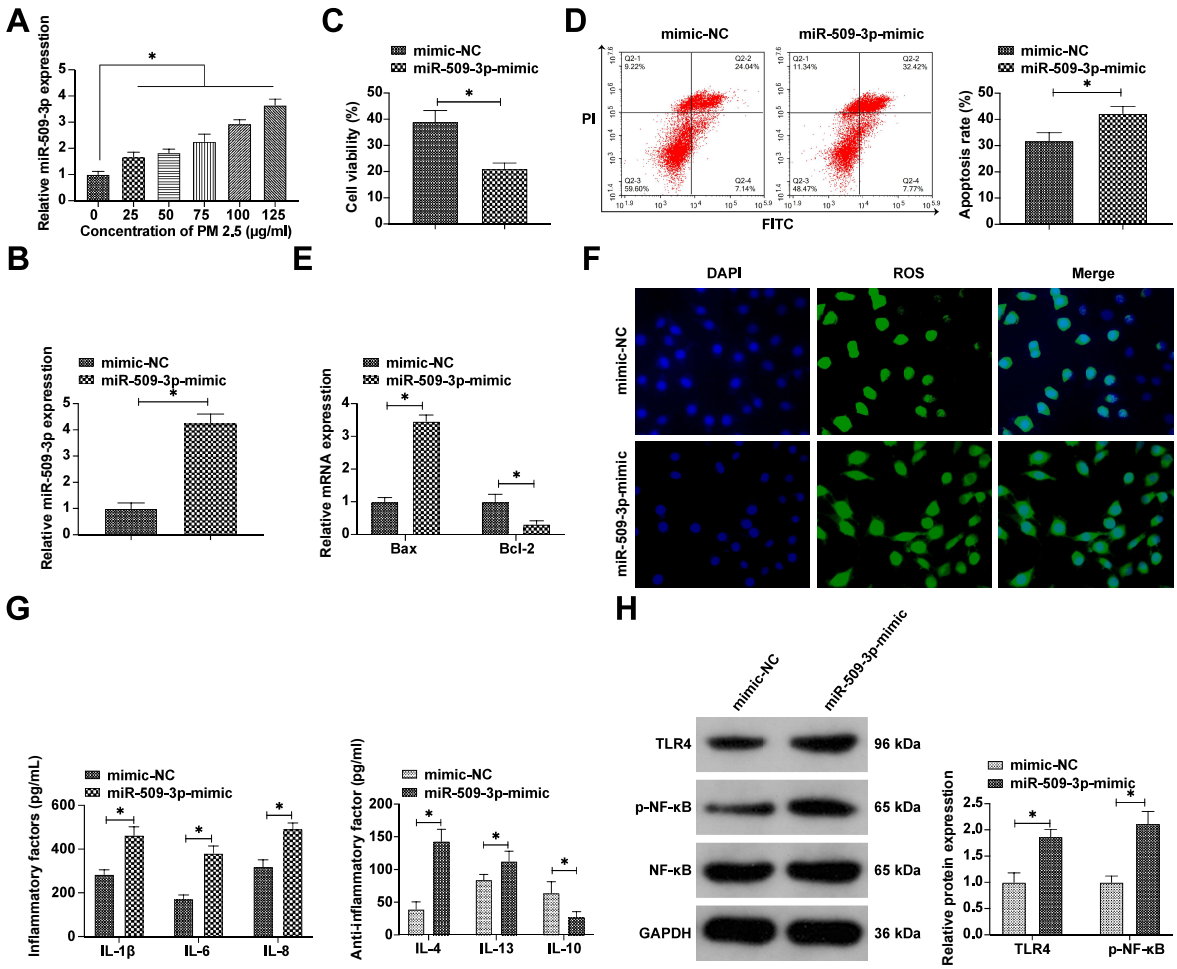

Fig. 3 Overexpression of miR-509-3p exacerbates $PM_{2.5}$-induced damage in BEAS-2B cells. A: MiR-509-3p expression in BEAS-2B cells post-$PM_{2.5}$ treatment at various concentrations; B: MiR-509-3p expression in BEAS-2B cells post-transfection with miR-509-3p-mimic; C: Cell viability in BEAS-2B cells post-miR-509-3p-mimic transfection; D: Apoptosis rates in BEAS-2B cells post-miR-509-3p-mimic transfection; E: Bax and Bcl-2 expression in BEAS-2B cells after miR-509-3p-mimic transfection; F: ROS levels in BEAS-2B cells post-miR-509-3p-mimic transfection; G: Inflammatory cytokine levels in BEAS-2B cells post-miR-509-3p-mimic transfection; H: TLR4 and phosphorylated NF-κB p65 expression in BEAS-2B cells post-miR-509-3p-mimic transfection. A, B, and E were assessed by RT-qPCR. C, D, F, G, and H were determined as mentioned in legend of Fig. 1. Values are mean ± SD ($n = 3$); * $p < 0.05$.

CircARF3 orchestrates $PM_{2.5}$-induced BEAS-2B cell injury via the miR-509-3p/CHD9 axis

Subsequently, we investigated the involvement of the miR-509-3p/CHD9 axis in the circARF3-mediated regulation of injury in BEAS-2B cells. Our findings revealed that overexpressing circARF3 or knocking down circARF3 respectively resulted in increased and decreased expression of CHD9. Intriguingly, the effects of circARF3 overexpression on CHD9 were reversed by CHD9 knockdown (Fig. 6A). Further experiments demonstrated that co-transfecting BEAS-2B cells with oe-circARF3 and si-CHD9 led to an increase in cellular viability and a decrease in apoptosis induced by circARF3 overexpression, effects that were negated by CHD9 knockdown (Fig. 6B,C). Additionally, overexpression of circARF3 was associated with reduced expression of the pro-apoptotic gene Bax and increased expression of the anti-apoptotic gene Bcl-2, which were restored to baseline levels following CHD9 knockdown (Fig. 6D). The suppressive effect of circARF3 overexpression on ROS production in BEAS-2B cells was also inhibited by knocking down CHD9 (Fig. 6E). ELISA and Western blot analyses indicated that the influence of circARF3 overexpression on pro-inflammatory and anti-inflammatory cytokines, as well as on phosphorylated NF-κB p65 and TLR4 protein expression, was reversed by CHD9 knockdown (Fig. 6F,G). These re-

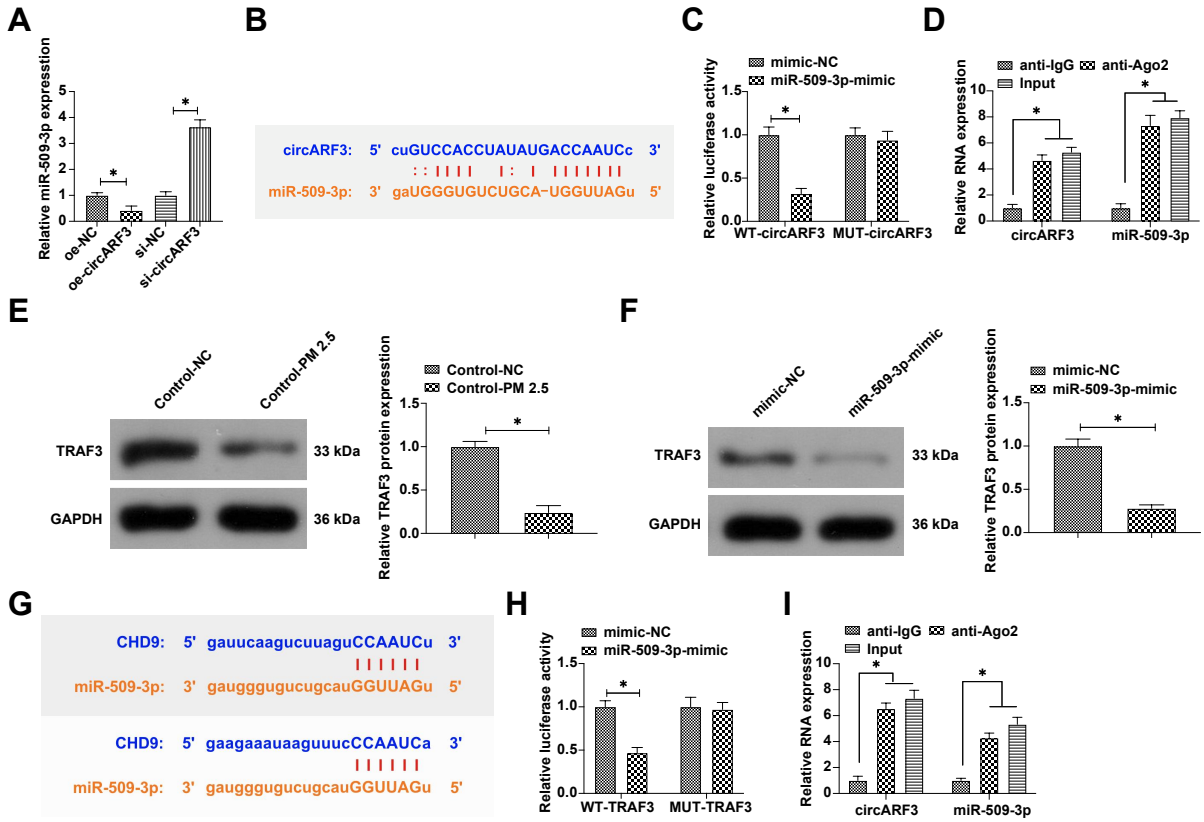

Fig. 4 CircARF3 and CHD9 as upstream and downstream regulators of miR-509-3p. A: MiR-509-3p expression in BEAS-2B cells post-transfection with oe/si-circARF3, determined by RT-qPCR; B: Predicted binding sites between circARF3 and miR-509-3p; C: Validation of the interaction between circARF3 and miR-509-3p; D: Confirmation of circARF3 and miR-509-3p interaction; E: CHD9 protein expression in BEAS-2B cells post-$PM_{2.5}$ exposure; F: CHD9 expression in BEAS-2B cells post-overexpression of miR-509-3p; G: Predicted binding sites between CHD9 and miR-509-3p; H: Validation of the interaction between CHD9 and miR-509-3p; I: Confirmation of CHD9 and miR-509-3p interaction. B and G, using website http://starbase.sysu.edu.cn/; C and H, by dual-luciferase reporter assay; D and I, through RIP experiment; E and F, by Western blot. Values are mean ± SD ($n = 3$); * $p < 0.05$.

sults suggest that circARF3 modulates $PM_{2.5}$-induced cellular damage through the miR-509-3p/CHD9 axis.

DISCUSSION

A burgeoning concern in environmental health research [25], $PM_{2.5}$ exposure can cause respiratory health problems not only through physical damage, but also through epigenetic changes in respiratory epithelial cells [26]. However, the intricate molecular mechanisms have remained largely elusive. Our study marks a significant advance in this field, revealing a critical role for circARF3 in counteracting the adverse effects of $PM_{2.5}$ exposure on bronchial epithelial cells. CircARF3 mediates this protective effect through a complex regulatory axis involving miR-509-3p and CHD9, highlighting a novel and complex molecular pathway for cellular defense against air pollution

Consistent with prior research [5, 27], our findings reiterate that $PM_{2.5}$ exposure leads to a decrease in cell viability and an increase in apoptosis in airway epithelial cells, and in our bronchial epithelial cell model, we observed this pattern in a dose-dependent manner. Notably, we discovered that the expression of circARF3 was correlated with the concentration of $PM_{2.5}$, but intriguingly, not with the duration of exposure. This could be attributed to the differences in the dynamics of $PM_{2.5}$ accumulation in *in vivo* environments as compared to controlled *in vitro* settings. Additionally, our observations revealed that a specific concentration of $PM_{2.5}$ not only increased ROS production but also activated the TLR4/NF-κB signaling pathway, a critical inflammatory cascade linked to air pollution exposure [28, 29].

Our study also aligns with emerging research underscoring the role of circRNAs in mediating respiratory damage caused by $PM_{2.5}$. For instance, high-throughput sequencing studies have indicated altered expression of non-coding RNAs, including circRNAs under $PM_{2.5}$ exposure [30]. In our research, we extended these insights by demonstrating that cir-

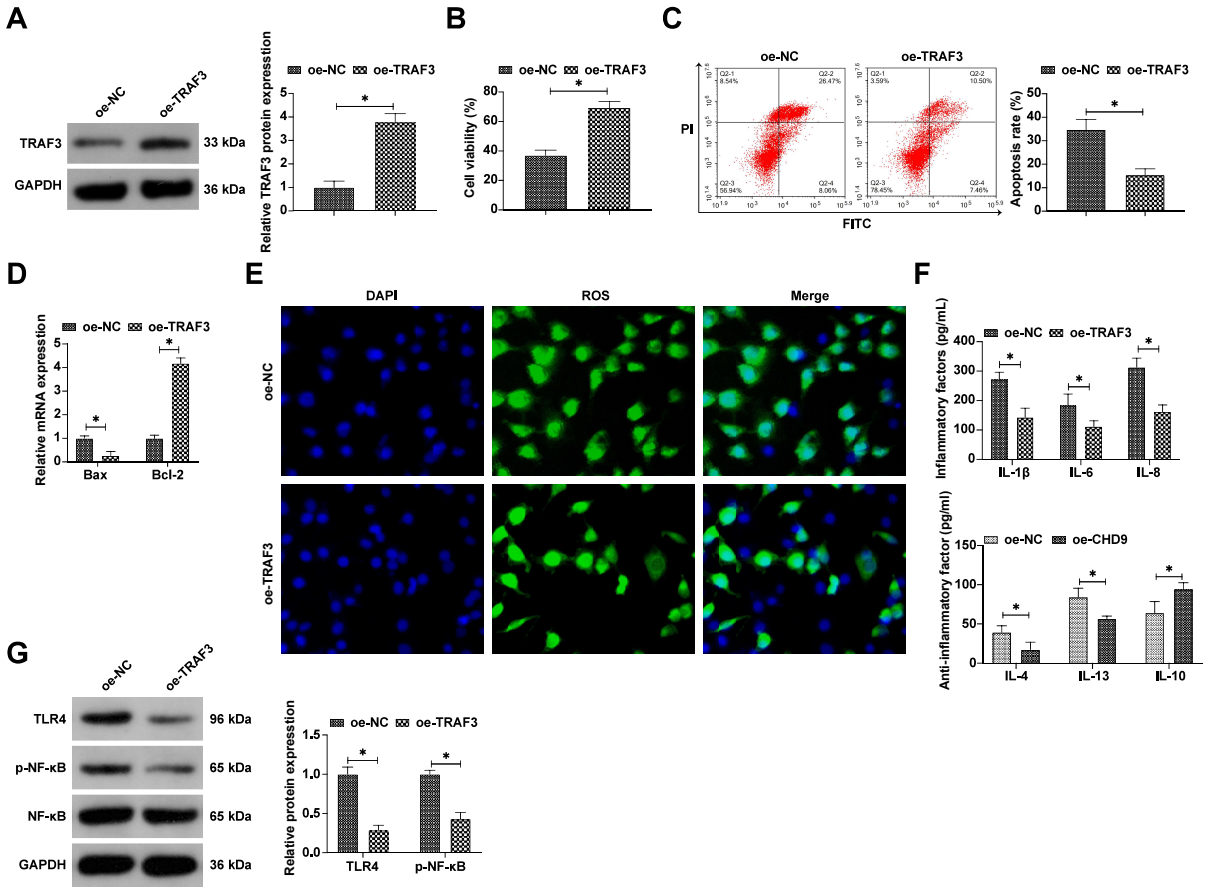

Fig. 5 Overexpression of CHD9 improves $PM_{2.5}$-induced damage in BEAS-2B cells. A: CHD9 expression in BEAS-2B cells post-transfection with oe-CHD9, analyzed by Western blot; B: Cell viability in BEAS-2B cells post-oe-CHD9 transfection; C: Apoptosis rates in BEAS-2B cells post-oe-CHD9 transfection; D: Bax and Bcl-2 expression in BEAS-2B cells post-oe-CHD9 transfection, determined by RT-qPCR; E: ROS levels in BEAS-2B cells post-oe-CHD9 transfection; F: Inflammatory cytokine levels in BEAS-2B cells post-oe-CHD9 transfection; G: TLR4 and phosphorylated NF-κB p65 expression in BEAS-2B cells post-oe-CHD9 transfection. B, C, E, F, and G were determined as mentioned in legend of Fig. 1. Values are mean ± SD ($n = 3$); * $p < 0.05$.

cARF3 overexpression significantly suppressed $PM_{2.5}$-induced apoptosis, inflammation, and oxidative stress in bronchial epithelial cells. This findings reinforced the anti-inflammatory potential of circARF3 and marked it as a promising biomarker for diagnosing diseases related to $PM_{2.5}$ exposure. Nevertheless, translating these *in vitro* findings into clinical or animal models requires further investigation, paving the way for translational research.

As part of our study, we examined CHD9, a member of the TRAF family known to influence the NF-κB pathway. Specifically, CHD9 degradation is pivotal in stabilizing NF-κB inducing kinase, leading to the nuclear translocation of NF-κB p65, a crucial step in inflammatory response modulation [31]. Our findings revealed that CHD9 overexpression significantly inhibited the TLR4/NF-κB pathway activation triggered by $PM_{2.5}$ exposure, consequently attenuating the inflammatory cascade. This overexpression also diminished ROS production and cellular apoptosis in bronchial epithelial cells. Intriguingly, the knockdown of CHD9 negated the protective effects of circARF3 against $PM_{2.5}$-induced damage, highlighting the role of circARF3 in regulating CHD9 expression and inhibiting the activation of the downstream TLR4/NF-κB inflammatory signaling.

The complex interaction of molecular events following $PM_{2.5}$ exposure was examined in our *in vitro* cellular model. This type of model, however, might not accurately depict physiological responses and intricate environmental interactions *in vivo*. Our study predominantly focused on cellular viability, apoptosis, ROS production, and inflammatory markers, potentially overlooking broader molecular and cellular responses. The roles of circARF3, miR-509-3p, and CHD9 in $PM_{2.5}$-induced bronchial epithelial cell injury,

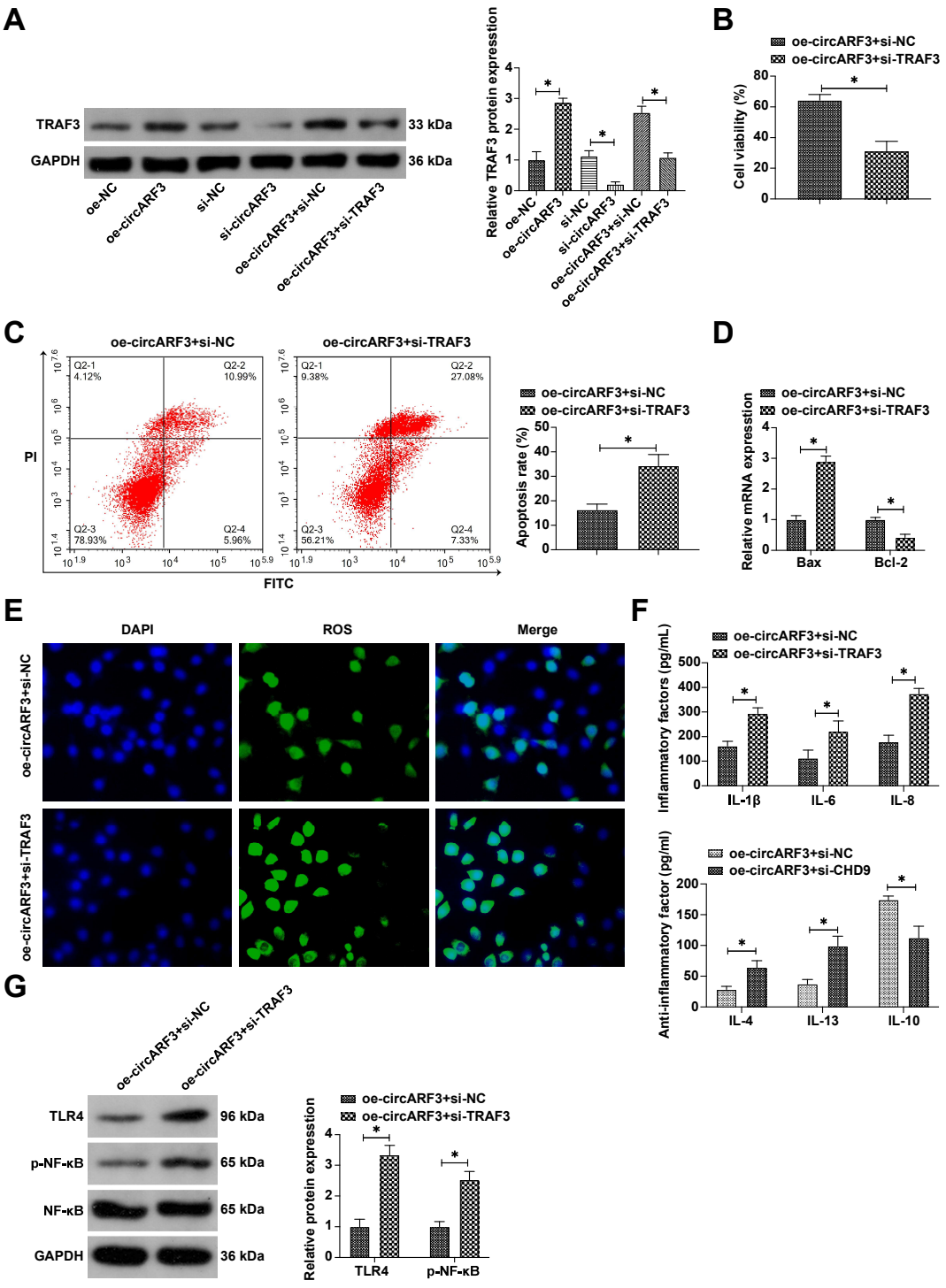

Fig. 6 circARF3 regulates $PM_{2.5}$-induced BEAS-2B cell injury via the miR-509-3p/CHD9 axis. A: CHD9 expression in BEAS-2B cells post-transfection with oe/si-circARF3 and co-transfection with si-CHD9, analyzed by Western blot; B: Cell viability in BEAS-2B cells post-co-transfection with oe-circARF3 and si-CHD9; C: Apoptosis rates in BEAS-2B cells post-co-transfection with oe-circARF3 and si-CHD9; D: Bax and Bcl-2 expression in BEAS-2B cells post-co-transfection with oe-circARF3 and si-CHD9, determined by RT-qPCR; E: ROS levels in BEAS-2B cells post-co-transfection with oe-circARF3 and si-CHD9; F: Inflammatory cytokine levels in BEAS-2B cells post-co-transfection with oe-circARF3 and si-CHD9; G: TLR4 and phosphorylated NF-κB p65 expression in BEAS-2B cells post-co-transfection with oe-circARF3 and si-CHD9. B, C, E, F, and G were determined as mentioned in legend of Fig. 1. Values are mean ± SD ($n = 3$); * $p < 0.05$.

while promising, require further exploration to establish their interactions and precise causal relationships in more complex biological systems. Future research, particularly in animal models, is essential to corroborate our findings and to gain a more comprehensive understanding of circARF3's function and mechanisms within an organismal context. Additionally, investigating the long-term impact of $PM_{2.5}$ exposure on the respiratory system and the specific role of circARF3 in chronic exposure scenarios could provide deeper insights into the pathogenesis of chronic respiratory conditions.

In conclusion, our study identifies circARF3 as a pivotal molecular entity in the landscape of $PM_{2.5}$-induced bronchial epithelial cell injury, operating through a complex interplay with miR-509-3p and CHD9. These insights offer novel avenues for therapeutic intervention in respiratory ailments associated with $PM_{2.5}$ exposure, enriching the current understanding of air pollution-related respiratory pathophysiology.

Appendix A. Supplementary data

Supplementary data associated with this article can be found at https://dx.doi.org/10.2306/scienceasia1513-1874.2025.057.

Acknowledgements: We appreciate funding from 2021 Changshu City Health Committee Science and Technology Plan Project (No: CSWS202121).

REFERENCES

1. Liu C, Chen R, Sera F, Vicedo-Cabrera A, Guo Y, Tong S, Coelho M, Saldiva P, et al (2019) Ambient particulate air pollution and daily mortality in 652 cities. *N Engl J Med* **381**, 705–715.
2. Beelen R, Raaschou-Nielsen O, Stafoggia M, Andersen Z, Weinmayr G, Hoffmann B, Wolf K, Samoli E, et al (2014) Effects of long-term exposure to air pollution on natural-cause mortality: an analysis of 22 European cohorts within the multicentre ESCAPE project. *Lancet* **383**, 785–795.
3. Raaschou-Nielsen O, Andersen Z, Beelen R, Samoli E, Stafoggia M, Weinmayr G, Hoffmann B, Fischer P, et al (2013) Air pollution and lung cancer incidence in 17 European cohorts: prospective analyses from the European Study of Cohorts for Air Pollution Effects (ESCAPE). *Lancet Oncol* **14**, 813–822.
4. Sun B, Song J, Wang Y, Jiang J, An Z, Li J, Zhang Y, Wang G, et al (2021) Associations of short-term PM exposures with nasal oxidative stress, inflammation and lung function impairment and modification by GSTT1-null genotype: A panel study of the retired adults. *Environ Pollut* **285**, 117215.
5. Fu Y, Li B, Yun J, Xu J, Meng Q, Li X, Chen R (2021) lncRNA SOX2-OT ceRNA network enhances the malignancy of long-term PM-exposed human bronchial epithelia. *Ecotoxicol Environ Saf* **217**, 112242.
6. Aztatzi-Aguilar O, Pardo-Osorio G, Uribe-Ramírez M, Narváez-Morales J, De Vizcaya-Ruiz A, Barbier O (2021) Acute kidney damage by PM exposure in a rat model. *Environ Toxicol Pharmacol* **83**, 103587.
7. Tao S, Xu Y, Chen M, Zhang H, Huang X, Li Z, Pan B, Peng R, et al (2021) Exposure to different fractions of diesel exhaust PM induces different levels of pulmonary inflammation and acute phase response. *Ecotoxicol Environ Saf* **210**, 111871.
8. Jiang M, Li D, Piao J, Li Y, Chen L, Li J, Yu D, Pi J, et al (2021) Nrf2 modulated the restriction of lung function via impairment of intrinsic autophagy upon real-ambient PM exposure. *J Hazard Mater* **408**, 124903.
9. Bozzoni I (2021) Widespread occurrence of circular RNA in eukaryotes. *Nat Rev Genet* **22**, 550–551.
10. Gao X, Xia X, Li F, Zhang M, Zhou H, Wu X, Zhong J, Zhao Z, et al (2021) Circular RNA-encoded oncogenic E-cadherin variant promotes glioblastoma tumorigenicity through activation of EGFR-STAT3 signalling. *Nat Cell Biol* **23**, 278–291.
11. Vausort M, Salgado-Somoza A, Zhang L, Leszek P, Scholz M, Teren A, Burkhardt R, Thiery J, et al (2016) Myocardial infarction-associated circular RNA predicting left ventricular dysfunction. *J Am Coll Cardiol* **68**, 1247–1248.
12. Dube U, Del-Aguila J, Li Z, Budde J, Jiang S, Hsu S, Ibanez L, Fernandez M, et al (2019) An atlas of cortical circular RNA expression in Alzheimer disease brains demonstrates clinical and pathological associations. *Nat Neurosci* **22**, 1903–1912.
13. Li J, Zhuo Z, Ren Z, Lid G (2023) Silencing circRNA TLK1 reduces endothelial cell injury in coronary heart disease. *ScienceAsia* **49**, 899–909.
14. Bai J, Deng J, Han Z, Cui Y, He R, Gu Y, Zhang Q (2021) CircRNA_0026344 via exosomal miR-21 regulation of Smad7 is involved in aberrant cross-talk of epithelium-fibroblasts during cigarette smoke-induced pulmonary fibrosis. *Toxicol Lett* **347**, 58–66.
15. Wang T, Wang P, Chen D, Xu Z, Yang L (2021) circARRDC3 contributes to interleukin 13 induced inflammatory cytokine and mucus production in nasal epithelial cells via the miR 375/KLF4 axis. *Mol Med Rep* **23**, 141.
16. Li M, Hua Q, Shao Y, Zeng H, Liu Y, Diao Q, Zhang H, Qiu M, et al (2020) Circular RNA circBbs9 promotes PM-induced lung inflammation in mice via NLRP3 inflammasome activation. *Environ Int* **143**, 105976.
17. Jia Y, Li X, Nan A, Zhang N, Chen L, Zhou H, Zhang H, Qiu M, et al (2020) Circular RNA 406961 interacts with ILF2 to regulate PM-induced inflammatory responses in human bronchial epithelial cells via activation of STAT3/JNK pathways. *Environ Int* **141**, 105755.
18. Zhang Z, Zhang T, Feng R, Huang H, Xia T, Sun C (2019) CircARF3 alleviates mitophagy-mediated inflammation by targeting miR-103/TRAF3 in mouse adipose tissue. *Mol Ther Nucleic Acids* **14**, 192–203.
19. Zusso M, Lunardi V, Franceschini D, Pagetta A, Lo R, Stifani S, Frigo AC, Giusti P, et al (2019) Ciprofloxacin and levofloxacin attenuate microglia inflammatory response via TLR4/NF-kB pathway. *J Neuroinflammation* **16**, 148.
20. Poma P (2020) NF-κB and disease. *Int J Mol Sci* **21**, 9181.
21. Hoesel B, Schmid JA (2013) The complexity of NF-κB signaling in inflammation and cancer. *Mol Cancer* **12**, 86.
22. Ramachandran S, Karp PH, Osterhaus SR, Jiang P, Wohlford-Lenane C, Lennox KA, Jacobi AM, Praekh K, et al (2013) Post-transcriptional regulation of cystic fi-

brosis transmembrane conductance regulator expression and function by microRNAs. *Am J Respir Cell Mol Biol* **49**, 544–551.

23. Lu CH, Yeh DW, Lai CY, Liu YL, Huang LR, Lee AY, Jin SC, Chuang TH (2018) USP17 mediates macrophage-promoted inflammation and stemness in lung cancer cells by regulating TRAF2/TRAF3 complex formation. *Oncogene* **37**, 6327–6340.
24. Sun Y, Zhou Y, Shi Y, Zhang Y, Liu K, Liang R, Sun P, Chang X, et al (2021) Expression of miRNA-29 in pancreatic beta cells promotes inflammation and diabetes via TRAF3. *Cell Rep* **34**, 108576.
25. Yang L, Li C, Tang X (2020) The impact of PM on the host defense of respiratory system. *Front Cell Dev Biol* **8**, 91.
26. Zhong Y, Liao J, Hu Y, Wang Y, Sun C, Zhang C, Wang G (2019) PM upregulates microRNA-146a-3p and induces M1 polarization in RAW264.7 cells by targeting sirtuin1. *Int J Med Sci* **16**, 384–393.
27. Cheng W, Lu J, Wang B, Sun L, Zhu B, Zhou F, Ding Z (2021) Inhibition of inflammation-induced injury and cell migration by coelonin and militarine in PM-exposed human lung alveolar epithelial A549 cells. *Eur J Pharmacol* **896**, 173931.
28. Ge C, Tan J, Zhong S, Lai L, Chen G, Zhao J, Yi C, Wang L, et al (2020) Nrf2 mitigates prolonged $PM_{2.5}$ exposure-triggered liver inflammation by positively regulating SIKE activity: Protection by Juglanin. *Redox Biol* **36**, 101645.
29. Chen X, Deng T, Huo T, Dong F, Deng J (2021) MiR-140-5p/TLR4 /NF-κB signaling pathway: Crucial role in inflammatory response in 16HBE cells induced by dust fall PM. *Ecotoxicol Environ Saf* **208**, 111414.
30. Zhong Y, Wang Y, Zhang C, Hu Y, Sun C, Liao J, Wang G (2019) Identification of long non-coding RNA and circular RNA in mice after intra-tracheal instillation with fine particulate matter. *Chemosphere* **235**, 519–526.
31. Bishop G, Stunz L, Hostager B (2018) TRAF3 as a multifaceted regulator of B lymphocyte survival and activation. *Front Immunol* **9**, 2161.

Appendix A. Supplementary data

Table S1 RT-qPCR primer sequence.

	Primer sequence (5′–3′)
GAPDH	Forward: 5′-CGCTTCACGAATTTGCGTGTCAT-3′ Reverse: 5′- GAAGATGGTGATGGGATTTC-3′
CircARF3	Forward: 5′- CCTAGTTGGATAAAGCAGCC-3′ Reverse: 5′- CCGACAGCAGGACCAGGTCC -3′
U6	Forward: 5′- CTCGCTTCGGCAGCACA-3′ Reverse: 5′- AACGCTTCACGAATTTGCGT-3′
MiR-509-3p	Forward: 5′-GATTCGCTTGATTGGTACGTCTGT -3′ Reverse: 5′- TATGCTTGTTCACGACACCTTCAC -3′